

---

# Spatiotemporal Attention for Multivariate Time Series Prediction and Interpretation

---

**Tryambak Gangopadhyay**

Department of Mechanical Engineering  
Iowa State University  
Ames, IA 50011  
tryambak@iastate.edu

**Sin Yong Tan**

Department of Mechanical Engineering  
Iowa State University  
Ames, IA 50011  
tsyong98@iastate.edu

**Zhanhong Jiang**

Data Sciences & Product Development  
Johnson Controls  
Milwaukee, WI 53202  
zhanhong.jiang@jci.com

**Rui Meng**

Department of Statistics  
University of California, Santa Cruz  
Santa Cruz, CA 95064  
rmeng1@ucsc.edu

**Soumik Sarkar**

Department of Mechanical Engineering  
Iowa State University  
Ames, IA 50011  
soumiks@iastate.edu

## Abstract

Multivariate time series modeling and prediction problems are abundant in many machine learning application domains. Accurate interpretation of such prediction outcomes from a machine learning model that explicitly captures temporal correlations can be a major benefit to the domain experts. In this context, temporal attention has been successfully applied to isolate the important time steps for the input time series. However, in multivariate time series problems, spatial interpretation is also critical to understand the contributions of different variables on the model outputs. We propose a novel deep learning architecture, called spatiotemporal attention mechanism (STAM) for simultaneous learning of the most important time steps and variables. STAM is a *causal* (i.e., only depends on past inputs and does not use future inputs) and *scalable* (i.e., scales well with an increase in the number of variables) approach that is comparable to the state-of-the-art models in terms of computational tractability. We demonstrate the performance of our models both on a popular public dataset as well as on a domain-specific dataset. When compared with the baseline models, the results show that STAM maintains state-of-the-art prediction accuracy while offering the benefit of accurate spatiotemporal interpretability. We validate the learned attention weights from a domain knowledge perspective for the real-world datasets.

## 1 Introduction

Multivariate time series analysis, classification and prediction capabilities are crucial for applications in different domains such as healthcare [1], financial markets [2], climate science [3, 4] and performance monitoring of engineering systems [5, 6]. Along with accuracy of decision-making, interpretability remains one of the important aspects for many real-life problems to build user trust and generate domain insights. Unfortunately however, often we find that there is a trade-off between the model complexity, accuracy and the ability to interpret the outcomes. Therefore, accurate predictive

modeling of multivariate time series coupled with interpretability mechanisms is still a hard technical challenge for the machine learning community.

Long Short Term Memory (LSTM) networks can capture the long-term temporal dependencies in complex multivariate time series [7] and have been used for a variety of applications [8, 9, 10]. In Encoder-Decoder model [11, 12], the information from all the input time-steps is encoded into a single fixed length vector, which is then used for decoding. Deep LSTM based encoder-decoder approach has been developed for multivariate time series forecasting problem without consideration of interpretability [13]. To address the bottleneck of using a fixed-length vector in encoder-decoder, a model based on attention was introduced which can automatically soft search for important parts of the input sequence in neural machine translation [14]. Inspired by this paper, attention mechanism based models have been developed for time series prediction [15, 16, 17, 18, 19, 20, 21, 22, 23]. We compare and contrast some of the notable works in Table 1. Some of the models are not causal, some are non-scalable and computationally intractable for large number of variables and with complicated interpretation mechanisms. Also, some models are only meant for single time-step prediction. Among the few spatiotemporal interpretability based approaches, no domain knowledge verification has been provided before. Also, previously developed approaches do not have any spatial attention to align directly with the output that hinders the ability to explicitly capture spatial correlations.

To address these limitations, we propose a novel spatiotemporal attention mechanism (STAM) for multivariate time-series prediction that provides meaningful spatiotemporal interpretations. The most important distinguishing features of our approach compared to the previous studies [15, 16, 17, 22] are the causal nature and that both the spatial and temporal attentions are aligned directly to the output variable. The model learns the temporal dependencies in data using LSTM layers in the encoder. At each output time-step, the model first soft searches for the most relevant time-steps and most significant variables. The model then predicts based on the computed spatial and temporal context vectors. For multivariate time-series, STAM can be applied in both regression and classification tasks with very minor modifications. The spatial and temporal interpretations can help users to better understand the contributions of different features and time-steps for prediction.

**Contributions.** We summarize the contributions of this work:

- (1) The proposed architecture STAM is novel for multiple time-step prediction in the context of interpretability for multivariate time-series problems. To the best of our knowledge, this is the first such work on attention-based time series models where the spatial and temporal attention weights are directly aligned to the output, in a causal and scalable (computationally tractable) manner.
- (2) The spatial and temporal attention mechanisms are jointly trained in a unified architecture to learn the temporal and spatial contributions. The learned interpretations are explained using domain knowledge for the real-world datasets. This model can be utilized for any application involving multivariate time series to provide spatiotemporal interpretability for the predictions.
- (3) STAM is interpretable while maintaining state-of-the-art prediction accuracy - STAM outperforms the baseline models in most of the experiments, while for a few experiments, STAM achieves comparable prediction accuracy.
- (4) We provide complexity analysis for our model and demonstrate that the complexity doesn't increase significantly after adding the spatial attention to the temporal one, especially when the length of input sequence is significantly larger than the number of input variables.

## 2 Related Work

RETAIN [15], based on a two-level neural attention model, detects influential patient visits and significant clinical variables for a binary classification task. In RETAIN, the spatial interpretation method is quite complicated, domain-specific and only meant for classification task. A dual-stage attention-based recurrent neural network (DA-RNN) [16] has spatial attention in the encoder layer and temporal attention in the decoder. DA-RNN is not causal as it depends also on future inputs during computation of the spatial weights in the encoding phase. Their work also suffers from lack of understanding of the attention weights from a domain knowledge perspective. AttentiveChrome [17] was developed to model and interpret dependencies among chromatin factors by using two levels of attention for a single output prediction (binary classification). The hierarchy of LSTM networks make AttentiveChrome non-scalable and computationally intractable in presence of large number of variables. Using bidirectional LSTMs to encode, the model is non-causal for time series domain

Table 1: Comparisons between existing and proposed mechanisms.

Method	Causal	Spa.Tem.Int.	Com.Tra.	Seq.Out.
RETAIN [15]	<span style="color:red">X</span>	<span style="color:green">✓</span>	<span style="color:green">✓</span>	<span style="color:red">X</span>
DA-RNN [16]	<span style="color:red">X</span>	<span style="color:green">✓</span>	<span style="color:green">✓</span>	<span style="color:red">X</span>
AttentiveChrome [17]	<span style="color:red">X</span>	<span style="color:green">✓</span>	<span style="color:red">X</span>	<span style="color:red">X</span>
SAnD [18]	<span style="color:red">X</span>	<span style="color:red">X</span>	<span style="color:green">✓</span>	<span style="color:red">X</span>
ICAtt [24]	<span style="color:green">✓</span>	<span style="color:red">X</span>	<span style="color:green">✓</span>	<span style="color:red">X</span>
DSTP-RNN [22]	<span style="color:red">X</span>	<span style="color:green">✓</span>	<span style="color:green">✓</span>	<span style="color:green">✓</span>
<b>STAM I</b> (ours)	<span style="color:green">✓</span>	<span style="color:green">✓</span>	<span style="color:green">✓</span>	<span style="color:green">✓</span>
<b>STAM II</b> (ours)	<span style="color:green">✓</span>	<span style="color:green">✓</span>	<span style="color:green">✓</span>	<span style="color:green">✓</span>

<sup>1</sup> **Spa.Tem.Int.:** Spatiotemporal Interpretability;

<sup>2</sup> **Com.Tra.:** Computationally Tractable (Scalable); <sup>3</sup> **Seq.Out.:** Sequence Output

applications. Transformer [25], based solely on attention mechanisms, has achieved state-of-the-art results for the machine translation task. But Transformer can only highlight sequential attention weights and will not be suitable for spatial interpretability in a causal way for time-series predictions. For clinical time-series modeling, attention based model SAnD [18] has been utilized inspired by the Transformer [25] model with some architectural modifications. Though computationally tractable, SAnD is not causal and does not provide spatiotemporal interpretability. Some attention based models [20, 21, 24] lacks in spatiotemporal interpretability having only spatial attention. Non-causal dual stage two-phase attention based LSTM model [22] has been utilized for multi time-step future prediction using multiple attention layers (also, at each encoding time-step) which complicates the interpretation. Other non-causal models developed in this domain include a multi-stage attention network [26] and a bidirectional LSTM network with temporal attention [27].

### 3 Preliminaries

#### 3.1 Notations and Problem Formulation

We introduce the notations to be used in this paper and formulate the problem we aim to study. Given  $N$  time series, we denote by  $\mathbf{X} = [\mathbf{x}^1, \mathbf{x}^2, \dots, \mathbf{x}^N]^\top \in \mathbb{R}^{N \times T_x}$ , the compact form of all time series, where  $T_x$  is the total input sequence length and  $\mathbf{x}^i = [x_1^i, x_2^i, \dots, x_{T_x}^i]^\top \in \mathbb{R}^{T_x}$ ,  $i \in \{1, 2, \dots, N\}$  signifies time series associated with each input variable. To represent all input variables at time step  $t \in \{1, 2, \dots, T_x\}$ , with a slight abuse of notation, we denote by  $\mathbf{x}_t = [x_t^1, x_t^2, \dots, x_t^N]^\top \in \mathbb{R}^N$  such that the compact form of all time series can also be expressed as  $\mathbf{X} = [\mathbf{x}_1, \mathbf{x}_2, \dots, \mathbf{x}_{T_x}]^\top$ . Analogously, we denote by  $\mathbf{y} \in \mathbb{R}^{T_y}$  the output time series for  $T_y$  time-steps, where  $\mathbf{y}_j \in \mathbb{R}$  is the output at time step  $j$ . For future time series prediction problems, given the historical information for  $T_x$  input time-steps, an employed sequence model aims at learning a (non)linear mapping for  $T_y$  future values of the output time series. To mathematically formulate this problem, we define  $\mathcal{F}(\cdot)$  as the mapping to be learned to obtain the prediction of  $\hat{\mathbf{y}}_j$  at output time-step  $j$ .

$$\hat{\mathbf{y}}_j = \mathcal{F}(\hat{\mathbf{y}}_1, \hat{\mathbf{y}}_2, \dots, \hat{\mathbf{y}}_{j-1}, \mathbf{x}_1, \mathbf{x}_2, \dots, \mathbf{x}_{T_x}) \quad (1)$$

In this paper, we aim to develop novel mapping functions  $\mathcal{F}$  in Eq. 1 that achieves highly comparable or better prediction accuracy while shedding light on both spatial and temporal relationships between input and output. Compared with most of the existing works mentioned in the last section, which only focused on either spatial or temporal interpretability, our work facilitates the accurate spatiotemporal interpretability that is quite crucial in time series prediction problems.

#### 3.2 Attention Mechanism

Various attention mechanisms have been proposed and popularly applied to different deep sequence models, such as RNN, GRU, and LSTM [28, 29]. We introduce here the existing attention mechanisms. We denote by  $\mathbf{h}_{t-1} \in \mathbb{R}^m$  and  $\mathbf{c}_{t-1} \in \mathbb{R}^m$  the encoder hidden state and cell state at time  $t-1$  respectively. It is well known that  $\mathbf{h}_t$  and  $\mathbf{c}_t$  can be calculated by leveraging the update laws of LSTM [30] which comprise of input, forget and output gates.

**Spatial Attention Mechanism.** The *spatial* attention mechanism can determine the relative contributions of different input variables in multivariate time series prediction. Recently, a number of papers

[16, 22, 26] have proposed to incorporate spatial attention in the encoding phase. Given the  $i$ -th attribute time series  $\mathbf{x}^i$  of length  $T_x$ , the spatial attention  $\beta_t^i$  at time-step  $t$  is computed as following.

$$e_t^i = \mathbf{v}_e^\top \tanh(W_e[\mathbf{h}_{t-1}; \mathbf{c}_{t-1}] + U_e \mathbf{x}^i), \quad \beta_t^i = \frac{\exp(e_t^i)}{\sum_{o=1}^N \exp(e_t^o)} \quad (2)$$

The raw input time series at time  $t$ ,  $\mathbf{x}_t$ , is then replaced by the *weighted* time series  $\hat{\mathbf{x}}_t$ , and with  $\hat{\mathbf{x}}_t$  as input to the encoder LSTM (function  $f_1$ ), the new states  $\mathbf{h}_t$  and  $\mathbf{c}_t$  are computed.

$$\hat{\mathbf{x}}_t = [\beta_t^1 x_t^1, \beta_t^2 x_t^2, \dots, \beta_t^N x_t^N]^\top, \quad (\mathbf{h}_t, \mathbf{c}_t) = f_1(\mathbf{h}_{t-1}, \mathbf{c}_{t-1}, \hat{\mathbf{x}}_t) \quad (3)$$

**Temporal Attention Mechanism.** The original *temporal* attention mechanism [14] was proposed to be used in the decoding phase after the encoder. At output time-step  $j$  of the decoder, the attention weight of each encoder hidden state is calculated by Eq. 4.

$$\alpha_j^t = \frac{\exp(a_j^t)}{\sum_{l=1}^T \exp(a_j^l)}, \quad \mathbf{s}_j = \sum_{t=1}^{T_x} \alpha_j^t \mathbf{h}_t. \quad (4)$$

The probability  $\alpha_j^t$  reflects how much the output  $\mathbf{y}_j$  is aligned to the input  $\mathbf{x}_t$ . The associated energy  $a_j^t$  is computed using an alignment model (feed forward neural network), which is a function of  $\mathbf{h}_t \in \mathbb{R}^m$  and previous decoder hidden state  $\mathbf{h}'_{j-1} \in \mathbb{R}^p$ . The *temporal context* vector  $\mathbf{s}_j$  is the input to the decoder at output time-step  $j$ . Intuitively, most temporal interpretability works [16, 17, 22, 26] have adopted this approach to compute the temporal attention weights.

**Limitations.** Recent works in multivariate time series prediction [16, 22, 26, 31] have developed different *spatiotemporal* attention mechanisms by incorporating the spatial attention into the encoder layer followed by temporal attention into the decoder layer, as done previously. Unfortunately, there exist two major limitations in these spatiotemporal attention mechanisms:

- (1) The *causality* is broken by using  $\mathbf{x}^i, 1 \leq i \leq N$  covering the whole length of  $T_x$  to compute the spatial attention weights (Eq. 2) which are used to calculate the *weighted* time series  $\hat{\mathbf{x}}_t$  (Eq. 3) at time-step  $t$ . The time-step  $t$  is ranging from 1 to  $T_x$  and for each  $t$ , the spatial attention weight calculations require future information ahead of  $t$ . Using  $\hat{\mathbf{x}}_t$  as input, the hidden state of the encoder LSTM  $\mathbf{h}_t$  is computed, which has implicit future information ahead of time-step  $t$ . It therefore affects temporal interpretability as well because the temporal attention alignment model is dependent on  $\mathbf{h}_t$ .
- (2) There is no such *spatial context* vector to align with the output time series directly, as in the temporal attention. Although the current approaches can measure the spatial importance in multivariate input time series based on Eq. 3, the spatial relationships between input and output can only be captured implicitly via the hidden states. Therefore, the existing approaches still lack accurate spatiotemporal interpretability.

## 4 Spatiotemporal Attention Mechanism (STAM)

We address the two limitations stated above by introducing a novel spatiotemporal attention mechanism (STAM) to 1) maintain the causality in the model and to 2) achieve accurate spatiotemporal interpretability. In this section, we propose and investigate the two variants of STAM (STAM I, STAM II) and their computational complexity. We illustrate the model variants in Fig. 1.

### 4.1 Spatial and Temporal Attentions

In STAM, we develop a spatiotemporal attention mechanism to come up with spatial and temporal context vectors to align directly with the output variable. The intuition behind such an idea is that instead of having the spatial attention in the encoder layer, a separate spatial attention is designed in parallel to the temporal attention in the decoder layer to simultaneously attend to the most relevant time steps and the most significant variables. Therefore, in STAM, both the spatial and temporal attentions align directly with the output. The inputs to the spatial and temporal attention are spatial and temporal embeddings respectively. The embeddings are generated independently. The spatial embeddings are obtained by using feed forward neural network for each feature  $\mathbf{x}^i = [x_1^i, x_2^i, \dots, x_{T_x}^i]^\top \in \mathbb{R}^{T_x}, i \in \{1, 2, \dots, N\}$ . From  $\mathbf{X} = [\mathbf{x}^1, \mathbf{x}^2, \dots, \mathbf{x}^N]^\top$ , the embeddings for all variables are computed as  $\mathbf{D} = [\mathbf{d}^1, \mathbf{d}^2, \dots, \mathbf{d}^N]^\top$ , where  $\mathbf{d}^i \in \mathbb{R}^m$ . Independently, the encoder consisting of two stacked LSTM layers, compute the temporal embeddings (hidden states) given

the input time series  $\mathbf{X} = [\mathbf{x}_1, \mathbf{x}_2, \dots, \mathbf{x}_{T_x}]^\top$ . At time-step  $t$ , the input to the encoder is  $\mathbf{x}_t = [x_t^1, x_t^2, \dots, x_t^N]^\top \in \mathbb{R}^N$ . The first LSTM layer in the encoder reads the input sequence in order from  $\mathbf{x}_1$  to  $\mathbf{x}_{T_x}$ . The hidden states returned by the first LSTM layer act as inputs to the second LSTM layer of the encoder. Using two LSTM layers, the encoder generates a sequence of hidden states, expressed as  $\mathbf{H} = [\mathbf{h}_1, \mathbf{h}_2, \dots, \mathbf{h}_{T_x}]^\top$ , where  $\mathbf{h}_t \in \mathbb{R}^m$ .

The hidden state and cell state in the decoder layer are denoted by  $\mathbf{h}' \in \mathbb{R}^p$  and  $\mathbf{c}' \in \mathbb{R}^p$ . A feed forward neural network is used as an alignment model to compute the spatial attention weights. At output time-step  $j$ , the  $i$ -th spatial attention weight  $\beta_j^i$  is calculated, where  $[\mathbf{h}'_{j-1}; \mathbf{d}^i] \in \mathbb{R}^{p+m}$  with  $\mathbf{h}'_{j-1} \in \mathbb{R}^p$  the previous hidden state of the decoder LSTM and  $\mathbf{d}^i \in \mathbb{R}^m$  the spatial embedding for  $i$ -th feature. The parameters to learn are  $W_e \in \mathbb{R}^{p+m}$  and  $b_e \in \mathbb{R}$ . We adopt the ReLU activation function instead of tanh due to slightly better results obtained through the empirical studies. We then calculate the spatial context vector using the spatial attention weights.

$$e_j^i = \text{ReLU}(W_e^\top [\mathbf{h}'_{j-1}; \mathbf{d}^i] + b_e), \quad \beta_j^i = \frac{\exp(e_j^i)}{\sum_{o=1}^N \exp(e_j^o)}, \quad \mathbf{g}_j = \sum_{i=1}^N \beta_j^i \mathbf{d}^i \quad (5)$$

For output time-step  $j$ , to get the temporal attention weight  $\alpha_j^t$  corresponding to the hidden state  $\mathbf{h}_t$ , the associated energy  $a_j^t$  is computed as follows:

$$a_j^t = \text{ReLU}(W_a^\top [\mathbf{h}'_{j-1}; \mathbf{h}_t] + b_a) \quad (6)$$

where  $[\mathbf{h}'_{j-1}; \mathbf{h}_t] \in \mathbb{R}^{p+m}$  with  $\mathbf{h}'_{j-1} \in \mathbb{R}^p$  the previous decoder hidden state and  $\mathbf{h}_t \in \mathbb{R}^m$  the temporal embedding for  $t$ -th input time-step. The parameters to learn are  $W_a \in \mathbb{R}^{p+m}$  and  $b_a \in \mathbb{R}$ . Thereafter, the attention weights  $\alpha_j^t$  for  $t \in \{1, 2, \dots, T_x\}$  are calculated followed by the temporal context vector  $\mathbf{s}_j$  according to Eq. 4. It should be noted that the spatial context vector  $\mathbf{g}_j$  and the temporal context vector  $\mathbf{s}_j$  are distinct at each time step.

## 4.2 STAM I

In STAM I, there is a single LSTM layer in the decoder. At output time-step  $j$ , the context vectors  $\mathbf{g}_j$  and  $\mathbf{s}_j$  are computed using the previous decoder hidden state  $\mathbf{h}'_{j-1}$  as described above. To align both the contexts with the output time series, we first concatenate these two vectors into  $[\mathbf{g}_j; \mathbf{s}_j] \in \mathbb{R}^{2m}$ . The concatenated dimension is reduced to  $\mathbf{r}_j \in \mathbb{R}^q$  using a feed forward neural network as shown in Eq. 7. We optimize the extent of this reduction through our experiments. Next we update  $\mathbf{r}_j$  by concatenating with output of the previous time-step  $\hat{\mathbf{y}}_{j-1}$ . The concatenation is denoted by  $\hat{\mathbf{r}}$ . It should be noted that the decoder output  $\hat{\mathbf{y}}_{j-1}$  is a scalar in time series prediction instead of a vector.

$$\mathbf{r}_j = \text{ReLU}(W_{GS}[\mathbf{g}_j; \mathbf{s}_j] + b_{GS}), \quad \hat{\mathbf{r}}_j = [\mathbf{r}_j; \hat{\mathbf{y}}_{j-1}] \quad (7)$$

where  $W_{GS} \in \mathbb{R}^{q \times 2m}$  and  $b_{GS} \in \mathbb{R}^q$  are parameters to learn. Instead of the real measurement, the prediction of the output time series is utilized through *non-teacher forcing* training approach, which enables the learning to be more robust. The decoder hidden state  $\mathbf{h}'_j$  and cell state  $\mathbf{c}'_j$  are updated by using  $\hat{\mathbf{r}}_j$  as input to the decoder LSTM (function  $f_2$ ):

$$(\mathbf{h}'_j, \mathbf{c}'_j) = f_2(\mathbf{h}'_{j-1}, \mathbf{c}'_{j-1}, \hat{\mathbf{r}}_j). \quad (8)$$

We can observe that the spatiotemporal context vector is aligned directly with the output variable enabling accurate interpretability, which will be shown empirically. Eq. 8 suggests that in STAM I, both the spatial and temporal attentions share the same decoder parameterized by a LSTM layer, which is due to the concatenation of the two context vectors. Next, we demonstrate the variant STAM II which uses two LSTM layers in the decoder.

## 4.3 STAM II

In STAM II, the spatial and temporal attentions rely on two different LSTM layers (denoted by  $\text{LSTM}_G$  and  $\text{LSTM}_S$ ) in the decoder. Therefore, the hidden state inputs also become different to the spatial and temporal attentions. For the purpose of presentation, we denote the hidden and cell states of the LSTM corresponding to the spatial context  $\mathbf{g}_j$  with  $*_G$ , where  $*$  indicates either hidden or cell state. The states are therefore denoted as  $\mathbf{h}'_G \in \mathbb{R}^p$  and  $\mathbf{c}'_G \in \mathbb{R}^p$ . At output time-step  $j$ , the input to the spatial attention (Eq. 5) is  $\mathbf{h}'_{G,j-1}$  to compute the spatial context vector  $\mathbf{g}_j$ . After dimension reduction using a feed forward neural network and concatenation with  $\hat{\mathbf{y}}_{j-1}$ ,  $\hat{\mathbf{r}}_{G,j}$  becomes the input to  $\text{LSTM}_G$  as follows:

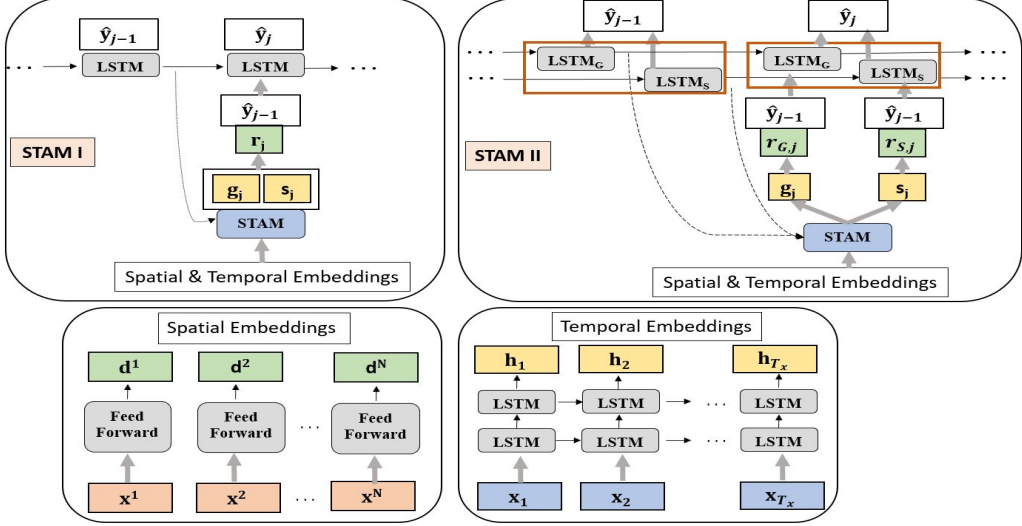


Figure 1: The illustration of the proposed model variants STAM I and STAM II attempting to compute the output  $\hat{y}_j$  at time step  $j$ .

$$\mathbf{r}_{G,j} = \text{ReLU}(W_G \mathbf{g}_j + b_G), \quad \hat{\mathbf{r}}_{G,j} = [\mathbf{r}_{G,j}; \hat{y}_{j-1}] \quad (9)$$

where  $W_G \in \mathbb{R}^{q \times m}$  and  $b_G \in \mathbb{R}^q$  are parameters to learn. Similarly, for the LSTM corresponding to the temporal context  $\mathbf{s}_j$ , the states are indicated with  $*_S$ . The hidden and cell states are denoted by  $\mathbf{h}'_S \in \mathbb{R}^p$  and  $\mathbf{c}'_S \in \mathbb{R}^p$  respectively. At output time-step  $j$ , the previous  $\text{LSTM}_S$  hidden state  $\mathbf{h}'_{S,j-1}$  is the input to the temporal attention (Eq. 6) to compute the temporal context vector  $\mathbf{s}_j$  (Eq. 4). After reducing the dimension reduction and concatenating with  $\hat{y}_{j-1}$ ,  $\hat{\mathbf{r}}_{S,j}$  becomes the input to  $\text{LSTM}_S$  as shown here:

$$\mathbf{r}_{S,j} = \text{ReLU}(W_S \mathbf{s}_j + b_S), \quad \hat{\mathbf{r}}_{S,j} = [\mathbf{r}_{S,j}; \hat{y}_{j-1}] \quad (10)$$

where  $W_S \in \mathbb{R}^{q \times m}$  and  $b_S \in \mathbb{R}^q$  are parameters to learn. The decoder hidden states and cell states are updated as:

$$(\mathbf{h}'_{G,j}, \mathbf{c}'_{G,j}) = f_3(\mathbf{h}'_{G,j-1}, \mathbf{c}'_{G,j-1}, \hat{\mathbf{r}}_{G,j}), \quad (\mathbf{h}'_{S,j}, \mathbf{c}'_{S,j}) = f_4(\mathbf{h}'_{S,j-1}, \mathbf{c}'_{S,j-1}, \hat{\mathbf{r}}_{S,j}) \quad (11)$$

where  $f_3$  and  $f_4$  are the nonlinear mappings of  $\text{LSTM}_G$  and  $\text{LSTM}_S$  respectively. Before prediction, the last step for STAM II is to unify the hidden state updates of the two LSTMs together by concatenating into  $[\mathbf{h}'_{G,j}; \mathbf{h}'_{S,j}]$ . Compared to STAM I, one extra LSTM layer is added to the decoder in STAM II to separately account for the spatial and temporal impact of input time series on the output or target time series.

#### 4.4 Complexity Analysis

STAM in a principled manner, mainly involves four modules: the encoder, the spatial attention, the temporal attention, and the decoder. Therefore, we omit some operations such as spatial embeddings and concatenation reduction for the context vectors. The encoders and decoders in both the variants are spanned by LSTM layers. Either STAM I or STAM II has two LSTM layers in the encoder. We first analyze the inference time complexity of the STAM I model having one LSTM layer in the decoder. We follow the similar way of the calculation as in [32]. As the state size of the encoder is  $m$  and that of the decoder is  $p$ , such a mechanism leads to the inference time complexity of  $\mathcal{O}(8(Nm + m^2 + 2m)T_x + (p + 2 + 2m)(N + T_x)T_y + 4T_y(p^2 + pq + 3p))$ , where  $q$  is the dimension of the context vector after dimension reduction. The first and third terms inside signify the computational complexity for the encoder and decoder respectively. The second term is for both the spatial and temporal attentions. Compared to the STAM I, which only concatenates two different context vectors together for producing the output, in STAM II the decoder module uses two LSTM layers separately to process the context vectors generated from the spatial and temporal attentions, respectively. This intuitively increases the computational complexity. Hence, taking into account all the four modules results in the inference time complexity of  $\mathcal{O}(8(Nm + m^2 + 2m)T_x + (p + 2 + 2m)(N + T_x)T_y + 8T_y(p^2 + pq + 3p))$ , which shows the complexity increment by  $4T_y(p^2 + pq + 3p)$  due to one extra LSTM layer in the decoder module of STAM II. We also observe this in the empirical results.

## 5 Experiments

### 5.1 Datasets

**Pollution Dataset:** We use the Beijing PM2.5 Data Set from the UCI Machine Learning Repository. It is an hourly dataset comprising the PM2.5 data of the US Embassy in Beijing and meteorological data from Beijing Capital International Airport [33]. For  $T_x$  input time-steps, we use 8 variables - pollution(PM2.5 concentration), dew point, temperature, pressure, combined wind direction, cumulated wind speed, cumulated hours of snow and cumulated hours of rain. We predict the pollution for the upcoming  $T_y$  time-steps. Keeping last 20% of the dataset for testing, the approximate sizes of the training, validation and test sets are 26,275, 8,758 and 8,759 respectively.

**Building Dataset:** We use a public multivariate time series dataset collected from an air handling unit in a building heating, ventilation and air-conditioning (HVAC) system [34]. This dataset consist of 9 variables - average zone temperature (Avg Zone Temp), outside air temperature (OAT,  $^{\circ}$ F), return air temperature (RAT,  $^{\circ}$ F), outside air damper command (OA Damper CMD), cooling valve command (Cool Valve CMD), discharge air temperature (DAT,  $^{\circ}$ F), supply fan speed command (Su Fan Speed CMD), discharge air static pressure (DA StaticP), and return fan speed command (Re Fan Speed CMD). With this multivariate input of  $T_x$  time-steps, the output is average zone temperature for upcoming  $T_y$  time-steps. The training, validation and test sizes are approximately 20,932, 6,977 and 6,978 respectively.

### 5.2 Baseline Models and Results

**Baseline Models:** For comparison of the empirical results, we use several baseline models: Epsilon-Support Vector Regression with Radial Basis Function kernel (SVR-RBF), Encoder-Decoder (Enc-Dec) model [11, 12], LSTM with temporal attention (LSTM-Att) model [14], and Dual-stage Attention Recurrent Neural Networks (DA-RNN) [16]. We try to optimize the hyper-parameters of all the baseline models as well including SVR-RBF which have shown improved results than in [27]. The optimized values of hidden state dimensions for the Enc-Dec, LSTM-Att and DA-RNN models are 32, 32 and 64 respectively. With this setting, the approximate number of trainable parameters for Enc-Dec, LSTM-Att and DA-RNN are 18,831, 19,120 and 57,764 respectively for  $T_x = 5$  and  $T_y = 3$ . Additional details of the baseline models are provided in the supplementary materials.

Table 2: *Empirical results for pollution dataset (with  $T_x = 5$ ,  $T_y = 4$ ) and building dataset (with  $T_x = 5$ ,  $T_y = 3$ ). Each model was trained three times, to obtain the average and standard deviation of each evaluation metric. Tr.Time/epoch: Train Time / epoch*

Model	Pollution Dataset			Building Dataset		
	RMSE	$R^2$ Score	Tr.Time / epoch	RMSE	$R^2$ Score	Tr.Time / epoch
SVR-RBF	48.14 $\pm$ 0.00	0.735 $\pm$ 0.00	11.96s	0.134 $\pm$ 0.000	0.987 $\pm$ 0.00	0.19s
Enc-Dec	48.04 $\pm$ 0.21	0.736 $\pm$ 0.00	6.18s	0.077 $\pm$ 0.019	0.996 $\pm$ 0.00	4.40s
LSTM-Att	47.96 $\pm$ 0.38	0.737 $\pm$ 0.00	6.79s	0.060 $\pm$ 0.005	0.998 $\pm$ 0.00	4.76s
DA-RNN	49.21 $\pm$ 0.11	0.723 $\pm$ 0.00	7.36s	0.060 $\pm$ 0.001	0.998 $\pm$ 0.00	5.18s
STAM I	<b>47.66<math>\pm</math>0.16</b>	<b>0.741<math>\pm</math>0.00</b>	7.15s	0.063 $\pm$ 0.002	0.997 $\pm$ 0.00	5.20s
STAM II	47.78 $\pm$ 0.40	0.739 $\pm$ 0.00	8.84s	<b>0.059<math>\pm</math>0.002</b>	<b>0.998<math>\pm</math>0.00</b>	5.94s

**Results:** We perform experiments to come up with the best set of hyper-parameters for training our STAM models. Keeping the hidden state dimensions of encoder and decoder same ( $m = p$ ) for simplicity, dimension of 32 gives better results in the experiments. We use Adam optimizer with learning rate of 0.001 and batch size of 256. To prevent overfitting, dropout layer (0.2) is used after each LSTM layer and each model is trained for 50 epochs. Through experiments, we optimize the input sequence length to  $T_x = 5$  and dimension reduction of context vectors to  $q = 4$  for both the datasets. The approximate number of trainable parameters for STAM I and STAM II are 19,761 and 24,733 respectively for  $T_x = 5$  and  $T_y = 3$ . We use three evaluation metrics: root mean square error (RMSE), mean absolute error (MAE), and coefficient of determination or R-squared score ( $R^2$ ). We utilize NVIDIA Titan RTX GPU for training our models. Table 2 presents the empirical results for both pollution and building datasets. The training time per epoch (the number of seconds to train a model once for the entire training set) are provided for each model, with the exception for SVR-RBF where the total training time is shown. We provide additional results for the MAE metric and the test time of models in the supplementary materials. From Table 2, STAM I and STAM II shows better performance than the baseline models for the pollution dataset. For the building

dataset, STAM II shows better performance than STAM I. There is a drastic difference in training and testing time for SVR-RBF model between pollution and building datasets. This is because SVR-RBF takes a lot more iterations to reach convergence and acceptable error threshold ( $\epsilon = 0.1$ ) for the pollution dataset as compared to the building dataset. Table 2 also shows that STAM is scalable and computationally tractable showing comparable training time to DA-RNN. Regarding prediction performance, STAM maintains high accuracy and outperforms the baseline models in most cases. Attention based time series models achieving comparable performance to that of the baseline models have been reported previously [15, 17]. Additionally, STAM provides the benefit of accurate spatiotemporal interpretability, which we describe next.

### 5.3 Discussion on Interpretability

The proposed STAM models have been empirically shown to outperform the baseline models. As mentioned before, attention based models typically experience a tradeoff between prediction accuracy and interpretability. In this section, we discuss how the proposed approaches enable accurate spatiotemporal interpretability. From Table 3, when the output variable at a future time-step  $T_y$  is *pollution*, the five most relevant variables from STAM results include itself, dew point, wind speed, hours of snow, and hours of rain, according to the spatial attention weights. Temperature, pressure and wind direction have comparatively smaller weights. As the pollution is measured by PM2.5 concentration, such spatial correlations obtained by STAM are in accord with the specific underlying relationships found in [35]. Intuitively, wind direction and pressure are not supposed to have strong correlations with pollution as PM2.5 refers to the atmospheric particulate matters which could be cleaned by weather conditions of snow or rain and blown away depending on the wind strength(speed) rather than direction. Dew point indicates the temperature to which air must be cooled to become saturated with water vapor. It has a slightly higher attention weight than temperature(air) as dew point approximately shows how moist the air would be, which can affect the movement of the atmospheric particles. The *temporal attention* weights are concentrated mostly in the last few time-steps (hours) of the input sequence decreasing from  $T_x = 5$  to  $T_x = 1$ . Intuitively, the output in a time series is also affected mostly by recent time-steps and the correlation usually decreases with increasing time lag.

Table 3: *Spatial attention weight distribution from STAM I (same as that from STAM II)*.

Pollution Dataset		Building Dataset	
Variables	Attention Weight (%)	Variables	Attention Weight (%)
<b>Pollution</b>	<b>13.43</b>	<b>Avg Zone Temp</b>	<b>11.76</b>
<b>Dew Point</b>	<b>11.02</b>	OAT	7.02
Temperature	10.64	RAT	7.48
Pressure	10.81	<b>OA Damper CMD</b>	<b>20.26</b>
Wind Direction	10.42	Cool Valve CMD	9.13
<b>Wind Speed</b>	<b>14.28</b>	<b>DAT</b>	<b>14.73</b>
<b>Hours of Snow</b>	<b>14.68</b>	Su Fan Speed CMD	8.99
<b>Hours of Rain</b>	<b>14.64</b>	DA StaticP	9.28
		<b>Re Fan Speed CMD</b>	<b>11.26</b>

For the Building Dataset, with the *average zone temperature* (Avg Zone Temp) as the output variable, the *temporal attention* weights are almost equally distributed across all the input time-steps, suggesting that most likely, the correlation is weakly depending on time in this case with a quite high sampling frequency (one minute). This is attributed to the slow thermal dynamics in the zone as well as the impact of the building mass absorbing heat to resist the quick change of the zone temperature. Table 3 shows the most relevant variables found by STAM are outside air damper command (OA Damper CMD), discharge air temperature (DAT), return fan speed command (Re Fan Speed CMD), and itself. Such correlations can be interpreted well by the domain knowledge (detailed physics provided in the supplementary section). First, the Avg Zone Temp is affected by DAT since these two variables have direct physics relationship based on the heat transfer equation and in most building systems, the discharge air is pumped to the zone directly in summer without reheating. Return air temperature (RAT) indicates the temperature of zone air circulated back to the central system and due to the summer time of data collection, it is similar to the outside air temperature (OAT). Since the return air has relatively higher level of CO<sub>2</sub>, only part of it is mixed with the fresh outside air to generate the mixed air, which is then cooled down by the cooling valve to become discharge air. Thus, how much fresh outside air and return air is required to maintain the indoor comfort are determined by the OA Damper CMD and Re Fan Speed CMD, respectively, which significantly affects the Avg Zone Temp. The cooling valve command (Cool Valve CMD) controlling the cooled water flow rate directly

affects the mixed air temperature instead of zone temperature, resulting in a smaller attention weight. The discharge air static pressure (DA StaticP) has more impact on the air flow rate than OAT and RAT. The supply fan speed command (Su Fan Speed CMD), which signifies a key indicator for the air flow rate, has its attention weight closer to that of DA StaticP.

## 6 Conclusion

Multivariate time series prediction has numerous applications in various domains of significant societal impact such as healthcare, financial markets, agriculture and climate science to name a few. Performance monitoring of human-engineered systems also utilizes multivariate sensor time series data to a great extent for enhanced efficiency, safety and security. In this paper, we propose a deep learning architecture that can effectively capture the temporal correlations in multivariate time series data and simultaneously provide accurate interpretations of the prediction outcomes. The temporal and spatial attentions are directly aligned with the output variable. Leveraging the spatial context vector facilitates better spatial correlation-based interpretations between the input and output variables.

Such spatial and temporal interpretations can help users to better understand the contributions of different features and time-steps for prediction. Therefore, we believe that the work presented here can be a great resource for the domain experts in different sectors who seek trustworthy (not just a black-box) machine learning tool for analyzing time series data. Scientists, engineers, medical professionals, farmers, policy makers and various other types of users can gain valuable insights by understanding the predictions from the perspective of 'what' and 'where' highlighted by our proposed model. Therefore, the proposed model, which is applicable to any type of multivariate time series data can help in data-driven decision-making in various parts of the society, well-beyond the machine learning community.

While the spatial and temporal correlations are captured based on the attention weights, one potential limitation is how much data is required to achieve it, which remains an open problem in this work. The required number of data points could depend on how prominent the underlying relationships are between the input and output variables in a dataset. In future, we plan to extend STAM to problems involving multiple output variables.

## Acknowledgement

This work has been supported in part by the U.S. Air Force Office of Scientific Research under the YIP grant FA9550-17-1-0220. Any opinions, findings and conclusions or recommendations expressed in this publication are those of the authors and do not necessarily reflect the views of the sponsoring agency.

## References

- [1] Mohammad Taha Bahadori and Zachary Chase Lipton. Temporal-clustering invariance in irregular healthcare time series. *arXiv preprint arXiv:1904.12206*, 2019.
- [2] Pierpaolo D’Urso, Livia De Giovanni, and Riccardo Massari. Trimmed fuzzy clustering of financial time series based on dynamic time warping. *Annals of Operations Research*, pages 1–17, 2019.
- [3] Manfred Mudelsee. Trend analysis of climate time series: A review of methods. *Earth-science reviews*, 190:310–322, 2019.
- [4] John T Abatzoglou, Solomon Z Dobrowski, and Sean A Parks. Multivariate climate departures have outpaced univariate changes across global lands. *Scientific reports*, 10(1):1–9, 2020.
- [5] Aurora Gonzalez-Vidal, Fernando Jimenez, and Antonio F Gomez-Skarmeta. A methodology for energy multivariate time series forecasting in smart buildings based on feature selection. *Energy and Buildings*, 196:71–82, 2019.
- [6] Chuxu Zhang, Dongjin Song, Yuncong Chen, Xinyang Feng, Cristian Lumezanu, Wei Cheng, Jingchao Ni, Bo Zong, Haifeng Chen, and Nitesh V Chawla. A deep neural network for unsupervised anomaly detection and diagnosis in multivariate time series data. In *Proceedings of the AAAI Conference on Artificial Intelligence*, volume 33, pages 1409–1416, 2019.

[7] Pankaj Malhotra, Lovekesh Vig, Gautam Shroff, and Puneet Agarwal. Long short term memory networks for anomaly detection in time series. In *European Symposium on Artificial Neural Networks, Computational Intelligence and Machine Learning. Bruges (Belgium)*, page 89. Presses universitaires de Louvain, 2015 April 22-24.

[8] Johnathon Shook, Linjiang Wu, Tryambak Gangopadhyay, Baskar Ganapathysubramanian, Soumik Sarkar, and Asheesh K Singh. Integrating genotype and weather variables for soybean yield prediction using deep learning. *bioRxiv*, 2018.

[9] Yuxiu Hua, Zhifeng Zhao, Rongpeng Li, Xianfu Chen, Zhiming Liu, and Honggang Zhang. Deep learning with long short-term memory for time series prediction. *IEEE Communications Magazine*, 57(6):114–119, 2019.

[10] Tryambak Gangopadhyay, Anthony Locurto, James B Michael, and Soumik Sarkar. Deep learning algorithms for detecting combustion instabilities. In *Dynamics and Control of Energy Systems*, pages 283–300. Springer, 2020.

[11] Kyunghyun Cho, Bart Van Merriënboer, Caglar Gulcehre, Dzmitry Bahdanau, Fethi Bougares, Holger Schwenk, and Yoshua Bengio. Learning phrase representations using rnn encoder-decoder for statistical machine translation. *arXiv preprint arXiv:1406.1078*, 2014.

[12] Ilya Sutskever, Oriol Vinyals, and Quoc V Le. Sequence to sequence learning with neural networks. In *Advances in neural information processing systems*, pages 3104–3112, 2014.

[13] Alaa Sagheer and Mostafa Kotb. Unsupervised pre-training of a deep lstm-based stacked autoencoder for multivariate time series forecasting problems. *Scientific Reports*, 9(1):1–16, 2019.

[14] Dzmitry Bahdanau, Kyunghyun Cho, and Yoshua Bengio. Neural machine translation by jointly learning to align and translate. *arXiv preprint arXiv:1409.0473*, 2014.

[15] Edward Choi, Mohammad Taha Bahadori, Jimeng Sun, Joshua Kulas, Andy Schuetz, and Walter Stewart. Retain: An interpretable predictive model for healthcare using reverse time attention mechanism. In *Advances in Neural Information Processing Systems*, pages 3504–3512, 2016.

[16] Yao Qin, Dongjin Song, Haifeng Chen, Wei Cheng, Guofei Jiang, and Garrison Cottrell. A dual-stage attention-based recurrent neural network for time series prediction. *arXiv preprint arXiv:1704.02971*, 2017.

[17] Ritambhara Singh, Jack Lanchantin, Arshdeep Sekhon, and Yanjun Qi. Attend and predict: Understanding gene regulation by selective attention on chromatin. In *Advances in neural information processing systems*, pages 6785–6795, 2017.

[18] Huan Song, Deepta Rajan, Jayaraman J Thiagarajan, and Andreas Spanias. Attend and diagnose: Clinical time series analysis using attention models. In *Thirty-second AAAI conference on artificial intelligence*, 2018.

[19] Tryambak Gangopadhyay, Sin Yong Tan, Genyi Huang, and Soumik Sarkar. Temporal attention and stacked lstms for multivariate time series prediction. 2018.

[20] Xuan Zhang, Xun Liang, Aakas Zhiyuli, Shusen Zhang, Rui Xu, and Bo Wu. At-lstm: An attention-based lstm model for financial time series prediction. In *IOP Conference Series: Materials Science and Engineering*, volume 569, page 052037. IOP Publishing, 2019.

[21] Youru Li, Zhenfeng Zhu, Deqiang Kong, Hua Han, and Yao Zhao. Ea-lstm: Evolutionary attention-based lstm for time series prediction. *Knowledge-Based Systems*, 181:104785, 2019.

[22] Yeqi Liu, Chuanyang Gong, Ling Yang, and Yingyi Chen. Dstp-rnn: A dual-stage two-phase attention-based recurrent neural network for long-term and multivariate time series prediction. *Expert Systems with Applications*, 143:113082, 2020.

[23] Johnathon Shook, Tryambak Gangopadhyay, Linjiang Wu, Baskar Ganapathysubramanian, Soumik Sarkar, and Asheesh K Singh. Crop yield prediction integrating genotype and weather variables using deep learning. *arXiv preprint arXiv:2006.13847*, 2020.

- [24] Aya Abdelsalam Ismail, Mohamed Gunady, Luiz Pessoa, Hector Corrada Bravo, and Soheil Feizi. Input-cell attention reduces vanishing saliency of recurrent neural networks. In *Advances in Neural Information Processing Systems*, pages 10813–10823, 2019.
- [25] Ashish Vaswani, Noam Shazeer, Niki Parmar, Jakob Uszkoreit, Llion Jones, Aidan N Gomez, Łukasz Kaiser, and Illia Polosukhin. Attention is all you need. In *Advances in neural information processing systems*, pages 5998–6008, 2017.
- [26] Jun Hu and Wendong Zheng. Multistage attention network for multivariate time series prediction. *Neurocomputing*, 383:122–137, 2020.
- [27] Shengdong Du, Tianrui Li, Yan Yang, and Shi-Jinn Horng. Multivariate time series forecasting via attention-based encoder-decoder framework. *Neurocomputing*, 2020.
- [28] Mingxing Zhang, Yang Yang, Yanli Ji, Ning Xie, and Fumin Shen. Recurrent attention network using spatial-temporal relations for action recognition. *Signal Processing*, 145:137–145, 2018.
- [29] Yequan Wang, Minlie Huang, Xiaoyan Zhu, and Li Zhao. Attention-based lstm for aspect-level sentiment classification. In *Proceedings of the 2016 conference on empirical methods in natural language processing*, pages 606–615, 2016.
- [30] Sepp Hochreiter and Jürgen Schmidhuber. Long short-term memory. *Neural computation*, 9(8):1735–1780, 1997.
- [31] Shuhei Yoshimi and Koji Eguchi. Forecasting corporate financial time series using multi-phase attention recurrent neural networks. 2020.
- [32] Dat Thanh Tran, Alexandros Iosifidis, Juho Kannainen, and Moncef Gabbouj. Temporal attention-augmented bilinear network for financial time-series data analysis. *IEEE transactions on neural networks and learning systems*, 30(5):1407–1418, 2018.
- [33] Xuan Liang, Tao Zou, Bin Guo, Shuo Li, Haozhe Zhang, Shuyi Zhang, Hui Huang, and Song Xi Chen. Assessing beijing’s pm2. 5 pollution: severity, weather impact, apec and winter heating. *Proc. R. Soc. A*, 471(2182):20150257, 2015.
- [34] U.S. Department of Energy (DOE). Long-term data on 3 office air handling units. <http://aiweb.techfak.uni-bielefeld.de/content/bworld-robot-control-software/>, July 21, 2015.
- [35] Zhongang Qi, Tianchun Wang, Guojie Song, Weisong Hu, Xi Li, and Zhongfei Zhang. Deep air learning: Interpolation, prediction, and feature analysis of fine-grained air quality. *IEEE Transactions on Knowledge and Data Engineering*, 30(12):2285–2297, 2018.

## Supplementary Materials

### S.1 Baseline Models

We use the following baseline models to compare the results with our proposed models STAM I and STAM II. We try to optimize the hyper-parameters of the baseline models.

**SVR-RBF:** Epsilon-Support Vector Regression with Radial Basis Function kernel. We optimize the hyper-parameters of SVR-RBF, especially epsilon. After choosing the optimal set of hyper-parameters, we observe that SVR-RBF shows improved performance than in [27] for the pollution dataset.

**Enc-Dec:** Encoder-Decoder model [11, 12]. Originally developed for neural machine translation, deep LSTM based encoder-decoder model has also been applied for multivariate time series prediction [13]. The Enc-Dec model comprises of encoder for the input sequence and decoder for the output sequence. The encoder encodes the input sequence into a fixed-length vector, which is used by the decoder to predict the output sequence. The whole encoder-decoder setup is trained jointly.

**LSTM-Att:** LSTM with temporal attention model. Proposed as an extension to the Encoder-Decoder model [11, 12], the attention based model [14] can automatically soft search for important parts of the input sequence. Instead of encoding the whole input sequence into a single fixed-length vector, the model encodes the input sequence into a sequence of vectors. During decoding, it adaptively chooses a subset of these vectors where the most relevant information is concentrated. Intuitively, similar approach like this has been adopted for temporal attention in time series prediction [17, 27].

Both the *Enc-Dec* and *LSTM-Att* models were originally developed for neural machine translation. For time series prediction, the output at each decoder time-step is a scalar instead of a vector. We modify both of these models accordingly using mean squared error as the loss. Similar to STAM I and STAM II, the decoder receives the information of the previous predicted output instead of the real measurement through non-teacher forcing training approach.

**DA-RNN:** Dual-stage Attention-based Recurrent Neural Networks [16]. It has spatial attention in the encoder layer, which computes a sequence of hidden states. As described in our main paper content, one of the limitations of DA-RNN is that it is not causal depending on the future inputs during the encoding phase. The temporal attention weights are computed in the decoding phase.

Table 4: Approximate number of trainable parameters with input sequence length,  $T_x = 5$  and output sequence length,  $T_y = 3$  for each baseline model (except SVR-RBF) and our proposed STAM I and STAM II models.

Model	Enc-Dec	LSTM-Att	DA-RNN	STAM I	STAM II
Number of Parameters	~18,831	~19,120	~57,764	~19,761	~24,733

### S.2 Results

In the main paper content (Table 2), we have presented the results for evaluation metrics root mean square error (RMSE) and coefficient of determination or R-squared score ( $R^2$ ) along with the training time details. Corresponding to that Table 2, we provide here the results for the mean absolute error (MAE) metric and the test time of the models. We also present some additional results for the pollution and building datasets.

### S.3 Interpretability Comparison

In the main paper content, we have presented the spatial weight distribution from STAM for the pollution and building datasets. We explained the learned interpretations using domain knowledge. We present here the spatial interpretations learned by DA-RNN in comparison to that learned by STAM in Table 10 and Fig. 2.

For the pollution dataset, when the output variable at future time-step  $T_y$  is *pollution*, the five most relevant variables highlighted by STAM include itself, dew point, wind speed, hours of snow, and hours of rain, according to the spatial attention weights. Temperature, pressure and wind direction have comparatively smaller weights. From Table 10 and Fig. 2, we observe that closely, similar interpretations are generated by DA-RNN as well.

Table 5: Empirical results for **pollution** dataset (with  $T_x = 5$ ,  $T_y = 4$ ). Each model was trained three times, to obtain the average and standard deviation of each evaluation metric. This table is the detailed version of the Table 2 in the main content.

Model	RMSE	MAE	$R^2$ Score	Train Time / epoch	Test Time
SVR-RBF	$48.135 \pm 0.000$	$31.890 \pm 0.000$	$0.735 \pm 0.000$	11.9545s	2.8225s
Enc-Dec	$48.043 \pm 0.209$	$35.817 \pm 10.587$	$0.736 \pm 0.002$	6.1780s	0.6083s
LSTM-Att	$47.957 \pm 0.377$	$30.730 \pm 0.448$	$0.737 \pm 0.004$	6.7892s	0.6425s
DA-RNN	$49.207 \pm 0.106$	$31.267 \pm 0.220$	$0.723 \pm 0.001$	7.3586s	0.6594s
STAM I	<b><math>47.658 \pm 0.155</math></b>	$30.080 \pm 0.673$	<b><math>0.741 \pm 0.002</math></b>	7.1524s	0.6444s
STAM II	$47.778 \pm 0.404$	<b><math>29.853 \pm 0.965</math></b>	$0.739 \pm 0.004$	8.8391s	0.8560s

Table 6: Empirical results for **building** dataset (with  $T_x = 5$ ,  $T_y = 3$ ). Each model was trained three times, to obtain the average and standard deviation of each evaluation metric. This table is the detailed version of the Table 2 in the main content.

Model	RMSE	MAE	$R^2$ Score	Train Time / epoch	Test Time
SVR-RBF	$0.1344 \pm 0.0000$	$0.1125 \pm 0.0000$	$0.9874 \pm 0.0000$	0.1945s	0.0324s
Enc-Dec	$0.0776 \pm 0.0189$	$0.0586 \pm 0.0207$	$0.9956 \pm 0.0022$	4.4036s	0.4195s
LSTM-Att	$0.0601 \pm 0.0045$	$0.0450 \pm 0.0039$	<b><math>0.9975 \pm 0.0004</math></b>	4.7635s	0.4186s
DA-RNN	$0.0600 \pm 0.0013$	$0.0408 \pm 0.0006$	<b><math>0.9975 \pm 0.0002</math></b>	5.1849s	0.4820s
STAM I	$0.0634 \pm 0.0017$	$0.0448 \pm 0.0002$	$0.9972 \pm 0.0002$	5.1991s	0.5330s
STAM II	<b><math>0.0599 \pm 0.0024</math></b>	<b><math>0.0415 \pm 0.0010</math></b>	<b><math>0.9975 \pm 0.0002</math></b>	5.9360s	0.5954s

For the building dataset, when the output variable at future time-step  $T_y$  is *average zone temperature* (Avg Zone Temp), the most relevant variables highlighted by STAM are outside air damper command (OA Damper CMD), discharge air temperature (DAT), return fan speed command (Re Fan Speed CMD), and itself. Using domain knowledge, these correlations can be interpreted well (provided in the main paper content). While STAM provides accurate interpretability, DA-RNN fails to do so in this case. As shown in Table 10 and Fig. 2, the weights learned by DA-RNN are roughly same for all the variables.

#### S.4 Overview of the Building Dataset

In this section, we provide the overview of the working mechanism of an airside heating, ventilation and air-conditioning (HVAC) in the building. Every building HVAC system can be roughly divided

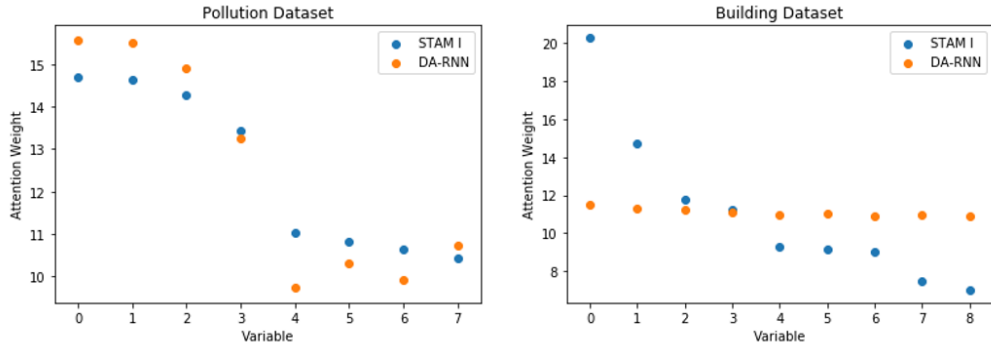


Figure 2: Plots of spatial attention weight distributions from STAM I and DA-RNN for pollution and building datasets. The variables are organized based on attention weights of STAM I (high to low).

Table 7: Empirical results for **pollution** dataset (with  $T_x = 5$ ,  $T_y = 3$ ). Each model was trained three times, to obtain the average and standard deviation of each evaluation metric.

Model	RMSE	MAE	$R^2$ Score
SVR-RBF	$42.399 \pm 0.000$	$27.917 \pm 0.000$	$0.795 \pm 0.000$
Enc-Dec	$42.105 \pm 0.155$	$25.432 \pm 0.477$	$0.798 \pm 0.002$
LSTM-Att	$41.739 \pm 0.564$	<b><math>25.683 \pm 0.969</math></b>	$0.801 \pm 0.005$
DA-RNN	$43.186 \pm 0.051$	$26.455 \pm 0.224$	$0.787 \pm 0.001$
STAM I	$41.873 \pm 0.200$	$25.851 \pm 0.785$	$0.800 \pm 0.002$
STAM II	<b><math>41.535 \pm 0.216</math></b>	$25.691 \pm 0.738$	<b><math>0.803 \pm 0.002</math></b>

Table 8: Empirical results for **pollution** dataset (with  $T_x = 5$ ,  $T_y = 1$ ). Each model was trained three times, to obtain the average and standard deviation of each evaluation metric.

Model	RMSE	MAE	$R^2$ Score
SVR-RBF	$26.740 \pm 0.000$	$17.941 \pm 0.000$	$0.918 \pm 0.000$
Enc-Dec	$25.521 \pm 0.514$	$13.879 \pm 0.445$	$0.926 \pm 0.000$
LSTM-Att	$23.682 \pm 0.342$	$13.381 \pm 0.801$	$0.936 \pm 0.002$
DA-RNN	$25.589 \pm 0.281$	$14.418 \pm 0.535$	$0.925 \pm 0.002$
STAM I	<b><math>23.517 \pm 0.133</math></b>	<b><math>13.182 \pm 0.122</math></b>	<b><math>0.937 \pm 0.001</math></b>
STAM II	$24.534 \pm 0.678$	$13.977 \pm 0.602$	$0.931 \pm 0.004$

into two sub-systems: airside HVAC system and waterside HVAC system. As the data used in our experiments is more related to the airside HVAC system, we omit the working mechanism of waterside HVAC system in this context.

Regarding the airside HVAC system, although it is essentially interacted with the waterside HVAC system, in terms of energy, it is on the demand side, which means that according to each zone's comfort requirement, the whole system generates the conditioned air to be supplied to the zones for satisfying the specific needs. We focus on the physical relationships qualitatively among the variables of the building dataset used in our experiments. We start with the definition of each variable.

#### S.4.1 Variables

**Average Zone Temperature (Avg Zone Temp,  $^{\circ}F$ ):** The temperature measured in an averaged way for a zone. This is because the local variable air volume supplying air to a zone can be located in different places inside the zone, depending on a specific building configuration. Thus, temperatures measured for different places inside the zone can be diverse. However, when collecting data, only one temperature is reported by averaging several slightly different zone temperatures.

**Outside Air Temperature (OAT,  $^{\circ}F$ ):** The temperature of the outdoor environment.

**Return Air Temperature (RAT,  $^{\circ}F$ ):** The temperature of the air returning from the zone.

**Outside Air Damper Command (OA Damper CMD):** The command signal of the damper position controlling the outside air. It is ranging from 0 – 100%, where 0% means that the damper is closed while 100% means that the damper is fully open.

**Cooling Valve Command (Cool Valve CMD):** The command signal of the valve position controlling the cooling water. It is ranging from 0 – 100%, where 0% means that the valve is closed while 100% means that the valve is fully open.

**Discharge Air Temperature (DAT,  $^{\circ}F$ ):** The temperature of discharge air, which is supplied to the zone.

**Supply Fan Speed Command (Su Fan Speed CMD):** The command signal of the supply fan to control how fast it runs. The supply fan is for pumping the discharge air.

Table 9: Empirical results for **building** dataset (with  $T_x = 5$ ,  $T_y = 2$ ). Each model was trained three times, to obtain the average and standard deviation of each evaluation metric.

Model	RMSE	MAE	$R^2$ Score
SVR-RBF	$0.1354 \pm 0.0000$	$0.1127 \pm 0.0000$	$0.9872 \pm 0.0000$
Enc-Dec	$0.0616 \pm 0.0061$	$0.0464 \pm 0.0057$	$0.9973 \pm 0.0005$
LSTM-Att	$0.0554 \pm 0.0024$	$0.0392 \pm 0.0025$	$0.9979 \pm 0.0002$
DA-RNN	$0.0548 \pm 0.0018$	$0.0400 \pm 0.0023$	$0.9979 \pm 0.0001$
STAM I	$0.0634 \pm 0.0018$	$0.0491 \pm 0.0026$	$0.9972 \pm 0.0002$
STAM II	<b><math>0.0528 \pm 0.0027</math></b>	<b><math>0.0367 \pm 0.0024</math></b>	<b><math>0.9980 \pm 0.0002</math></b>

Table 10: Spatial attention weight distributions from STAM I and DA-RNN (STAM II has similar weight distribution as STAM I).

Pollution Dataset			Building Dataset		
Variables	Attention Weight (%)		Variables	Attention Weight (%)	
	STAM I	DA-RNN		STAM I	DA-RNN
<b>Pollution</b>	<b>13.43</b>	<b>13.26</b>	<b>Avg Zone Temp</b>	<b>11.76</b>	<b>11.22</b>
<b>Dew Point</b>	<b>11.02</b>	9.75	OAT	7.02	10.88
Temperature	10.64	9.93	RAT	7.48	10.99
Pressure	10.81	10.30	<b>OA Damper CMD</b>	<b>20.26</b>	<b>11.53</b>
Wind Direction	10.42	10.74	Cool Valve CMD	9.13	11.00
<b>Wind Speed</b>	<b>14.28</b>	<b>14.91</b>	<b>DAT</b>	<b>14.73</b>	<b>11.32</b>
<b>Hours of Snow</b>	<b>14.68</b>	<b>15.55</b>	Su Fan Speed CMD	8.99	10.90
<b>Hours of Rain</b>	<b>14.64</b>	<b>15.49</b>	DA StaticP	9.28	10.96
			<b>Re Fan Speed CMD</b>	<b>11.26</b>	<b>11.12</b>

**Discharge Air Static Pressure (DA StaticP):** The static pressure of the discharge air.

**Return Fan Speed Command (Re Fan Speed CMD):** The command signal of the return fan to control how fast it runs. The return fan facilitates to circulate back the air to the central airside system.

#### S.4.2 Working Mechanism of the Airside HVAC System

Before introducing how the airside HVAC system works, we first mention two notations that will be used next. The first one is called air-handling unit (AHU) and the second one is aforementioned variable air volume (VAV). Typically, AHU generates the conditioned air for each zone. For each zone, its local VAV will reheat the conditioned air based on different comfort requirements and seasons (e.g., cooling season and heating season). As the data used in the experiments is collected from the cooling season, we focus only on how to cool down the zone temperature. We ignore any heating for the zone here.

When the fresh outside air is taken into the system by the AHU, at the same time, part of the return air from thermal zone(s) is circulated back to the AHU. Part of the return air is pumped out of the system as the exhaust air. One could reuse the total return air, but it would cause the ventilation issue as the CO<sub>2</sub> level keeps increasing. The reason of not using the refreshed outside air entirely is due to the energy saving, particularly for the winter (heating season). The outside air and return air is mixed in the AHU to become the mixed air.

Due to the cooling season, the mixed air temperature is quite high such that it cannot be provided directly to thermal zone(s). Then the cooling water comes to play. Before reaching the supply fan, the mixed air passes a coil system in the AHU. Since it is the cooling season, the cooling coil is activated to cool down the mixed air to become the discharge air. Hence, the discharge air is pumped by the

supply fan to the thermal zone(s). Before entering each thermal zone, depending on the record of the thermostat, the reheat coil on the VAV is activated or not. In cooling season, this is not usual, but also relies on different climates. After the discharge air enters into the thermal zone, it helps regulate the zone temperature to the reference temperature set by the thermostat. The air from the thermal zone(s) is pumped by the return air fan back to the central AHU system. This process is repeated in the airside HVAC system.